

The valence band energy spectrum of HgTe quantum wells with inverted band structures

G. M. Minkov,¹ V. Ya. Aleshkin,² O. E. Rut,¹ A. A. Sherstobitov,¹
A. V. Germanenko,¹ S. A. Dvoretzki,³ and N. N. Mikhailov^{3,4}

¹*Institute of Natural Sciences and Mathematics, Ural Federal University, 620002 Ekaterinburg, Russia*

²*Institute for Physics of Microstructures RAS, Nizhny Novgorod, Russia*

³*Institute of Semiconductor Physics RAS, 630090 Novosibirsk, Russia*

⁴*Novosibirsk State University, Novosibirsk 630090, Russia*

(Dated: September 24, 2018)

The energy spectrum of the valence band in HgTe/Cd_xHg_{1-x}Te quantum wells with a width (8 – 20) nm has been studied experimentally by magnetotransport effects and theoretically in framework 4-bands kP -method. Comparison of the Hall density with the density found from period of the Shubnikov-de Haas (SdH) oscillations clearly shows that the degeneracy of states of the top of the valence band is equal to 2 at the hole density $p < 5.5 \times 10^{11} \text{ cm}^{-2}$. Such degeneracy does not agree with the calculations of the spectrum performed within the framework of the 4-bands kP -method for symmetric quantum wells. These calculations show that the top of the valence band consists of four spin-degenerate extremes located at $k \neq 0$ (valleys) which gives the total degeneracy $K = 8$. It is shown that taking into account the “mixing of states” at the interfaces leads to the removal of the spin degeneracy that reduces the degeneracy to $K = 4$. Accounting for any additional asymmetry, for example, due to the difference in the mixing parameters at the interfaces, the different broadening of the boundaries of the well, etc, leads to reduction of the valleys degeneracy, making $K = 2$. It is noteworthy that for our case two-fold degeneracy occurs due to degeneracy of two single-spin valleys. The hole effective mass (m_h) determined from analysis of the temperature dependence of the amplitude of the SdH oscillations show that m_h is equal to $(0.25 \pm 0.02) m_0$ and weakly increases with the hole density. Such a value of m_h and its dependence on the hole density are in a good agreement with the calculated effective mass.

I. INTRODUCTION

The quantum wells in heterostructures HgTe/Cd_xHg_{1-x}Te have a number of unusual properties compared to quantum wells based on semiconductors with non-zero band gap. The reason for this is the “negative” band gap of gapless semiconductor HgTe in which Γ_6 band, forming a conduction band in conventional semiconductors, is located below the Γ_8 band, which in conventional semiconductors forms the valence band. Great attention is now paid to the study of topological states arising in such wells (see recent paper [1]). Knowledge of the energy spectrum of two-dimensional (2D) carriers is required for reliable interpretation of all phenomena and it has been studied in the last decade, both theoretically [2–7] and experimentally [8–14]. However, quite a lot of differences between the experimental data and the results of the calculations has been accumulated to date. First of all it refers to the spectrum of the top of valence band in the structures with quantum well width $d > (7.5 - 8) \text{ nm}$ [15–18]. The multi-band kP -calculations predict for such a case the nonmonotone E versus k dependence and the existence of four local maxima (valleys) at $k \neq 0$ and so the eight-fold degeneracy of these states (two-fold spin degeneracy, $s = 2$, and four-fold valley degeneracy, $v = 4$). However, such a degeneracy was not justified experimentally.

So, it should be recognized that the band spectrum of these structures cannot be considered well established

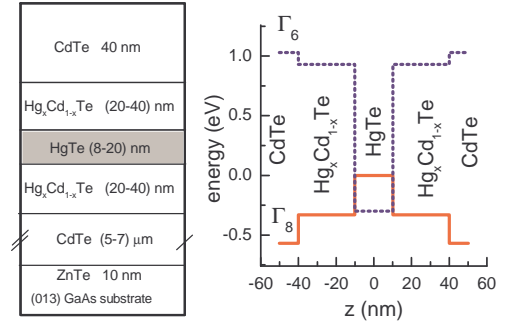


Figure 1. (Color online) Sketch and energy diagram of the structures investigated.

at the moment despite the large number of papers devoted to the study of HgTe/Cd_xHg_{1-x}Te quantum well heterostructures. In this paper, we present the results of experimental study of the magnetotransport in the heterostructures with the HgTe quantum wells with d from 8.3 nm to 20.4 nm, within a wide hole density range. The comparison of the Hall density and density found from the SdH oscillations clearly shows that the states near the top of valence band are two-fold degenerate within whole studied range of hole density and quantum well width. It is shown that a hole effective mass (m_h) found from the temperature dependence of the amplitude of SdH oscillations is about $(0.25 \pm 0.02) m_0$ at density $(1 - 2) \times 10^{11} \text{ cm}^{-2}$ and slightly increases with

the increasing hole density (m_0 is the free electron mass). To understand and interpret the experimental data we have calculated the energy spectrum using a 4-band Kane Hamiltonian. We show that taking into account the interface inversion asymmetry and any additional asymmetry, for example, due to the difference in the mixing parameters at the interfaces, the different broadening of the boundaries of the well, etc., explains the two-fold degeneracy of the states and gives quantitative agreement with the value of the hole effective mass and its density dependence.

II. EXPERIMENT

Our HgTe quantum wells were realized on the basis of HgTe/Cd_xHg_{1-x}Te ($x = 0.5-0.7$) heterostructure grown by molecular beam epitaxy on GaAs substrate with the (013) surface orientation [19]. The nominal widths of the quantum wells under study were $d = (8.3 - 20.4)$ nm. The samples were mesa etched into standard Hall bars of 0.5 mm width with the distance between the potential probes of 0.5 mm. To change and control the electron and hole densities in the quantum well (n and p , respectively), the field-effect transistors were fabricated with parylene as an insulator and aluminium as a gate electrode. The measurements were performed at temperature (1.3 – 4.2) K in the magnetic field up to 6 T. For each heterostructure, several samples were fabricated and studied. The sketch and the energy diagram of the structure investigated are shown in Fig. 1.

The parameters of the structures investigated are presented in the Table I. The main results for all the structures investigated are close to each other, therefore, as an example, let us consider in more detail the data obtained for the structure H1529 with $d = 8.3$ nm.

First, let us consider the behavior of the transverse (ρ_{xy}) and longitudinal (ρ_{xx}) resistivity within classical magnetic fields at different gate voltages (V_g). As seen from Fig. 2(a), $\rho_{xy}(B)$ changes the sign when the gate voltage changes. The value of ρ_{xy} linearly depends on magnetic field in $B \lesssim 1$ T within hole conductivity range (when $V_g < -1$ V) and in $B < (0.4 - 0.5)$ T within electron conductivity range (that corresponds to $V_g > +2$ V). (An exception is the structures with $d = 15$ nm and 20.4 nm where two-types conductivity is observed in magnetic field $B < 0.1$ T due to overlapping of the conduction and valence bands.) The gate voltage dependencies of the Hall density of the holes, $p_H = 1/eR_H(1 \text{ T})$, and electron density, $n_H = -1/eR_H(0.2 \text{ T})$, plotted in Fig. 2(b) show that the rate of change of the density of the electrons and holes, $-dn_H/dV_g$ and dp_H/dV_g , respectively, are close to each other and they are well described by the dependence $(1.6 \times 10^{11} - 7 \times 10^{10} V_g, \text{ V}), \text{ cm}^{-2}$ over the whole gate voltage range. It should be noted that the measurements of the capacitance (C) between the gate electrode and two-dimensional gas in the quantum well for the same sample give the value of $(1/e)dQ/dV_g =$

Table I. The parameters of heterostructures under study

| number | structure | d (nm) | type |
|--------|-----------|----------|----------|
| 1 | H1529 | 8.3 | p |
| 2 | H725 | 8.3 | p, n^a |
| 3 | HT71 | 9.5 | p, n^a |
| 4 | H1524 | 10 | n |
| 5 | H1312 | 15 | p |
| 6 | H1114 | 20.4 | p |

^a After illumination.

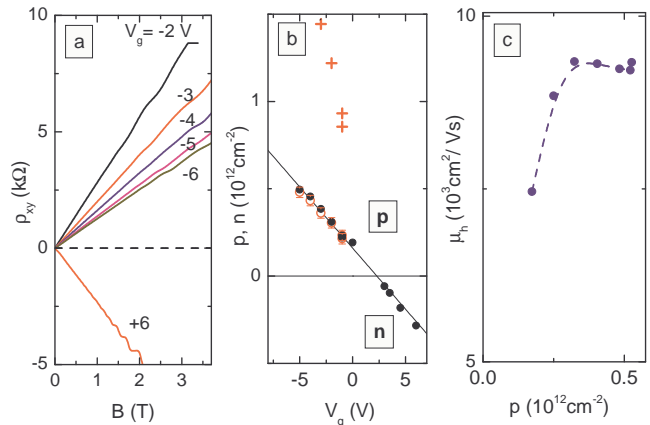


Figure 2. (Color online) (a) – The magnetic field dependencies of ρ_{xy} for some V_g values. (b) – The gate voltage dependence of the carriers density. The solid circles are the Hall density for holes $p_H = 1/eR_H(B = 1 \text{ T})$ and for electrons $n_H = -1/eR_H(B = 0.2 \text{ T})$. The crosses and empty circles are the hole density found from SdH oscillations for the degeneracy of the Landau levels (spin and valleys) 8 and 2 (crosses and circles, respectively). The solid line is carrier density found from capacitance between the 2D gas and gate electrode as $C(V_g^{\text{CNP}} - V_g)/eS_g$, where V_g^{CNP} is the gate voltage corresponding to charge neutrality point. (c) – The density dependence of the hole mobility. $T = 1.4 \text{ K}$.

$C/S_g = (7 \pm 0.1) \times 10^{10} \text{ cm}^{-2}/\text{V}$ (where S_g is the gate area). This value within experimental accuracy coincides with dn/dV_g and $-dp/dV_g$ found from the Hall measurements (the quantum capacitance gives contribution less than 1.5 percent).

So, $1/e|R_H|$ gives the density of the holes and electrons. The values of the hole mobility are large enough, $\mu_h = (7.5 - 8.5) \times 10^3 \text{ cm}^2/\text{Vs}$ [see Fig. 2(c)] and as Fig. 3(a) shows the SdH oscillations are observed at $T = 1.4 \text{ K}$. It is seen that some distortion of the oscillations starts to be observed in magnetic fields higher than $\approx 2.5 \text{ T}$. We assume, that this is due to the complex spectrum of the valence band in magnetic field, therefore we restrict ourselves for further consideration to the range of relatively low magnetic fields $B < 2.5 \text{ T}$. In Fig. 3(b), we have plotted the positions of the maxima of ρ_{xx} at different V_g values. One can see that the maxima shift to

the higher fields with the growing hole density when V_g becomes more negative. The data are well extrapolated to $V_g \simeq 2.3$ V at $B = 0$, i.e., to the V_g value, which corresponds to the charge neutrality point [compare Fig. 2(b) and Fig. 3(b)].

Now let us find the hole density from the SdH oscillations. For the case when the number of undistorted oscillations is not large, it is more reliable to determine their frequency in the reciprocal magnetic field from the fitting of the experimental curves to the Lifshits-Kosevich formula [20] rather than from the Fourier spectrum:

$$\frac{\rho_{xx}(B, T) - \rho_{xx}(0, T)}{\rho_{xx}(0, T)} \propto A(B, T) \cos\left(\frac{2\pi f}{B}\right) \quad (1)$$

with

$$A(B, T) = \exp\left(-\frac{\Delta}{\hbar\omega_c}\right) \frac{2\pi^2 k_B T}{\hbar\omega_c} / \sinh\left(\frac{2\pi^2 k_B T}{\hbar\omega_c}\right), \quad (2)$$

where f is the oscillations frequency in the reciprocal magnetic field, $\omega_c = eB/m$, m is effective mass, k_B is the Boltzmann constant, Δ is the broadening of the Landau levels (LL). An example of such a fitting procedure for $V_g = -5$ V within the magnetic field range (1.2 – 2.5) T is shown in Fig. 3(a) by the solid line.

To find the carrier density from the oscillations frequency f , one should know the spin and valley degeneracy, $K = s + v$, of the Landau levels:

$$p_{s\&H} = f \frac{e}{h} \times K. \quad (3)$$

The most straightforward way to determine K is based on analysis of the positions of the minima of ρ_{xx} in reciprocal magnetic field $1/B_{min}$ plotted as function of the oscillation number N [see Fig. 3(c)]. Really, the minima of ρ_{xx} occur in those fields, when the integer numbers of Landau levels are filled. The number of states in non-degenerate LL is $(e/h)B$ therefore at carrier density p , the filling factor will be equal to $\nu = p / [(e/h)B]$, so for integer ν [that corresponds to the minima in $\rho_{xx}(B)$] $1/B_{min}(N) = (e/h)K \times N/p$ [21].

Above, we have shown that the hole density is equal to p_H , therefore we have plotted in Fig. 3(c) the dependences $1/B_{min}(N) = (e/h) \times KN/p_H$ for different values of K . It is evident that the experimental values of $1/B_{min}(N)$ coincide with $(e/h) \times KN/p_H$ with $K = 2$ only. The hole density found from the frequency of the SdH oscillations using the degeneracy $K = 2$ are shown for all V_g values in Fig. 2(b). One can see that it coincides with Q/e determined from the capacitance measurements and with p_H over the whole density range. So, all the above data and their analysis show that the states of the top of valence band at hole density less than $5 \times 10^{11} \text{ cm}^{-2}$ are two-fold degenerate.

Another important parameter of the spectrum is the hole effective mass m_h . The value of m_h can be found from the temperature dependence of the amplitude of SdH oscillations. As an example, the oscillations of

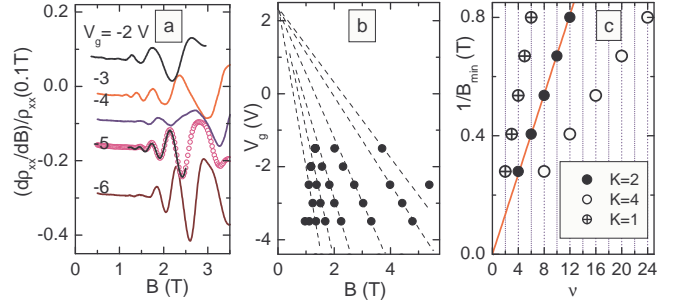


Figure 3. (Color online) (a) – The magnetic field dependences of $(d\rho_{xx}/dB)/\rho_{xx}(0.1 \text{ T})$ at different V_g , $T = 1.4$ K. The solid line for $V_g = -5$ V is fit to the Lifshits-Kosevich formula, Eq. (1). (b) – The positions of the maxima of ρ_{xx} in coordinates (B, V_g) . The dashed lines are provided as a guide for the eye. (c) – The points are the positions of minima of ρ_{xx} in inverse magnetic field, $1/B_{min}$, as a function of the filling factor for the different degeneracy of LL. The solid line is $(e/h) \times (N/p_H)$.

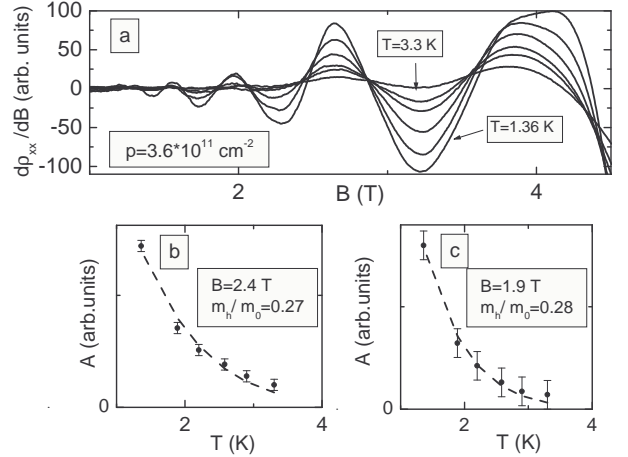


Figure 4. (Color online) (a) – the magnetic field dependences of $d\rho_{xx}/dB$ taken at different temperatures at $p = 3.6 \times 10^{11} \text{ cm}^{-2}$. (b) and (c) – The amplitude of the oscillations at different temperatures for $B = 2.4$ T and 1.9 T, respectively (symbols). The dashed curves are the results of the best fit to Eq. (2) with m_h/m_0 as the fitting parameter.

$d\rho_{xx}/dB$ at hole density $3.6 \times 10^{11} \text{ cm}^{-2}$ measured at different temperatures are presented in Fig. 4(a). To exclude the monotone contribution, analysis of temperature behavior of $d\rho_{xx}(B)/dB$ instead of $\rho_{xx}(B)$ is more reliable for such studies. The temperature dependences of the oscillations amplitude at two magnetic fields are shown in Figs. 4(b) and 4(c). They are well described by Eq. (2) with the hole effective mass $m_h = (0.27-0.28)m_0$. It should be noted that the use of Eq. (2) for determination of the effective mass presumes that the broadening Δ is independent of temperature. To check the validity of this assumption we have determined Δ at different temperatures from the magnetic field depen-

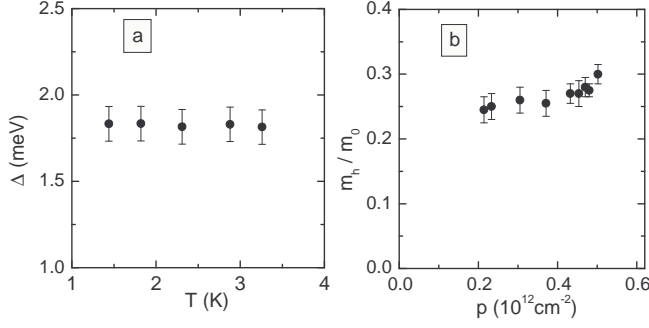


Figure 5. (Color online) (a) – The broadening Δ for different temperatures at $p = 3.6 \times 10^{11} \text{ cm}^{-2}$. (b) – The values of the hole effective mass found at different hole densities.

dencies of the oscillations amplitude. Figure 5(a) demonstrates that Δ really is independent of T in our case.

The values of the hole effective mass were determined for all the structures investigated with d from 8.3 nm to 20.4 nm at different hole densities. These results are collected in Fig. 6. It is evident that: (i) the hole effective mass is independent of the quantum well width within experimental accuracy, (ii) $m_h = (0.22 \pm 0.03) m_0$ at hole density $p \simeq (1 - 2) \times 10^{11} \text{ cm}^{-2}$, (iii) it weakly increases with the hole density.

III. THE CALCULATIONS OF THE ENERGY SPECTRUM OF THE VALENCE BAND AND DISCUSSION

This section is devoted to theoretical consideration of the electron spectrum in HgTe quantum well.

A. The energy spectrum of the valence band of the well with [013] orientation

The band structure was calculated using a 4-band Kane Hamiltonian. For the quantum well grown on the plane (013) the explicit form of the Hamiltonian including deformation terms is given in [22]. Calculation of the wave functions and electron spectrum was carried out for the superlattice with a large period when barriers virtually nontransparent. In this method, one can use periodic boundary conditions for the electron wave function (corresponding to the center of the Brillouin zone in the superlattice) and expand the wave function in a series:

$$\begin{aligned} \psi_j(x, y, z) &= \exp(ik_x x + ik_y y) \\ &\times \sum_{l=-N_{max}}^{l=N_{max}} C_l(k_x, k_y) \exp\left(\frac{2i\pi z l}{d_{sl}}\right) \\ &= \exp(ik_x x + ik_y y) \varphi_j(k_x, k_y, z) \end{aligned} \quad (4)$$

where the index j denotes the component of the wave function, k_x and k_y are components of the electron wave

vector in the plane of the quantum well (x and y axes are chosen along the [100] and [031] directions, respectively), d_{sl} is the superlattice period, $C_l(k_x, k_y)$ are the expansion coefficients. With this approach, finding the electron spectrum and the wave functions reduces to finding the eigenvalues and eigenvectors of the matrix $8(2N_{max}+1) \times 8(2N_{max}+1)$. In the calculation, the value $N_{max} = 20$ was used. Check with $N_{max} = 30$ showed practically identical results. We used in calculations the parameters for $\text{Hg}_{1-x}\text{Cd}_x\text{Te}$ from Ref. [4]. Parameters to describe the deformation contribution to the Hamiltonian were taken from Ref. [23].

Let us consider the calculated spectrum of the valence band in the quantum well with $d = 8.3 \text{ nm}$ for which the experimental results were presented in Figs. 2–6. Figure 7 shows that the top of the valence band consists of 4 local extremes (valleys), which are located at $k \neq 0$. The E versus k dependencies for three directions [100], [031] and direction which passes through maximum (labeled as [diagonal]) are presented in Fig. 8(a). The dashed lines in this figure divide the energy into three regions: (i) within the region 1, there are 4 closed isoenergy contours. It means that the states are 8-fold degenerate with taking into account the spin degeneracy; (ii) within the region 2, there are 2 closed isoenergy contours, which arise after the merger of the two pairs nearest valleys and the states are 4-fold degenerated; (iii) within the region 3, there are 2 concentric contours.

The dependence of the hole density on the Fermi energy for $p < 2 \times 10^{12} \text{ cm}^{-2}$ is plotted in Fig. 8(b). The hole density p was calculated as $p = svS_1(E_F)/(2\pi)^2$, where $S_1(E_F)$ is the area of the single closed contour at energy E_F in k space. For this case $s = 2$ while $v = 4$ within the Fermi energy range (20.5 – 18.0) meV and $v = 2$ for lower energy when two valleys are merged. This figure shows that over whole studied density range ($p < 5 \times 10^{11} \text{ cm}^{-2}$) there are 4 isolated isoenergy con-

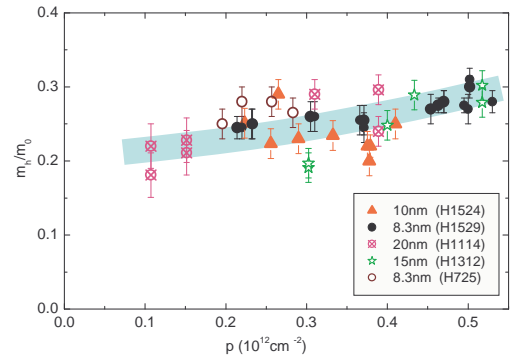


Figure 6. (Color online) The values of hole effective mass measured in all the structures investigated within whole density range. The calculated dependence of m_h with different parameters is presented by the wide semitransparent line (see Section III C).

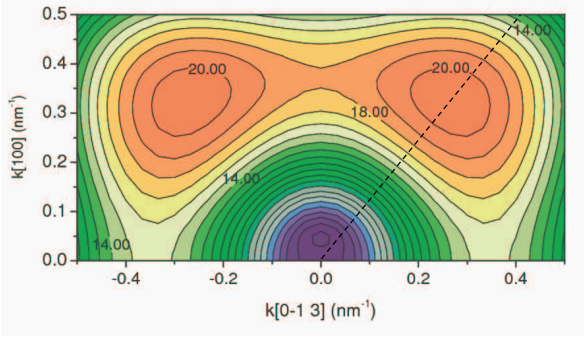


Figure 7. (Color online) The isoenergy contours of the top of valence band. Orientation of substrate is (013), width of the well is equal to 8.3 nm. We show half of the picture, the second part is a mirror image. The energy is measured from $E(k=0)$. The step is 1 meV. The energies for some contours are shown in plot. The dashed line shows the direction which passes through the maximum of $E(\mathbf{k})$.

At this point it should be noted that all the information on the spectrum was obtained from the oscillations in the magnetic field. Therefore, for comparison of the theoretical calculations with experiment one needs to know the energies of the Landau levels $E_N(B)$ for such spectrum. We use quasiclassical quantization rule which for quantization by a magnetic field is reduced to replacement $S_1 \rightarrow 2\pi(N+1/2)/L_H^2$, where $L_H = \sqrt{\hbar/eB}$ is the magnetic length, $N = 0, 1, 2, \dots$. So, the spin and valley degeneracy of the Landau levels coincides with the degeneracy of the spectrum at $B = 0$ in the valence band top. The energy distance between nearest Landau levels ($\hbar\omega_c$) is equal to $\hbar\omega_c = 2\pi(eB/\hbar)(dS_1/dE)^{-1}$ and the effective mass is $m = (\hbar^2/2\pi)dS_1/dE$. Namely this

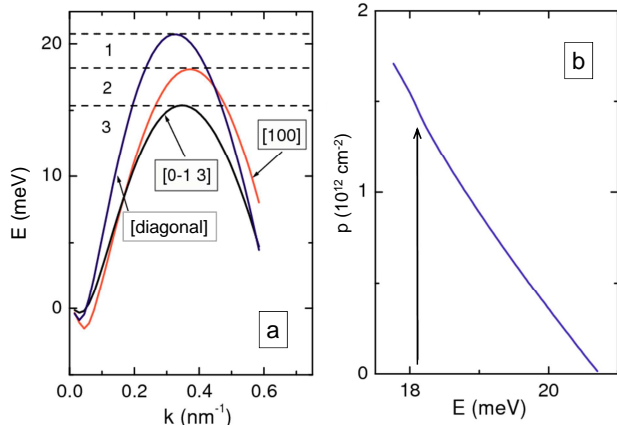


Figure 8. (Color online) (a) – The dependencies $E(k)$ for three directions: [100], [013] and [diagonal] one, which passes through the maximum of $E(\mathbf{k})$. (b) – The dependence of hole density on the Fermi energy. The arrow shows the density of holes at which the two nearby valleys are merged.

4(c)] [24].

Thus, the theoretical calculation predicts 8-fold degeneracy of the valence band states while experimental data give 2-fold degeneracy [25].

What factors were not taken into account in the above calculation? First and foremost is the lack of inversion symmetry in the heterostructures based on A_3B_5 , A_2B_6 semiconductors. It was shown [7, 26, 27] that interface inversion asymmetry (IIA) significantly changes the energy spectrum of HgTe quantum well, especially the top of the valence band.

B. The energy spectrum of the valence band with taking into account IIA

To take into account the IIA we used an additional term in the Hamiltonian, which is suggested by E. Ivchenko [29]. This term leads to “the mixing of the states” at the boundaries and in case when the normal to the quantum well is along to the [013] direction, is as follows

$$H_i = \frac{dU}{dz} \frac{1}{\sqrt{3}} \times \begin{pmatrix} 0 & 0 & 0 & 0 & 0 & 0 & 0 & 0 \\ 0 & 0 & 0 & 0 & 0 & 0 & 0 & 0 \\ 0 & 0 & \frac{3}{5} & -i\frac{4}{5} & 0 & -\frac{3\sqrt{2}}{10} & i\frac{4\sqrt{2}}{5} & \frac{3\sqrt{6}}{10} \\ 0 & 0 & \frac{3}{5} & 0 & 0 & -i\frac{4}{5} & 0 & \frac{3\sqrt{6}}{10} \\ 0 & 0 & i\frac{4}{5} & 0 & 0 & -\frac{3}{5} & \frac{3\sqrt{6}}{10} & 0 \\ 0 & 0 & 0 & i\frac{4}{5} & -\frac{3}{5} & 0 & i\frac{4\sqrt{2}}{5} & -\frac{3\sqrt{2}}{10} \\ 0 & 0 & -\frac{3\sqrt{2}}{10} & 0 & \frac{3\sqrt{6}}{10} & -i\frac{4\sqrt{2}}{5} & 0 & 0 \\ 0 & 0 & -i\frac{4\sqrt{2}}{5} & \frac{3\sqrt{6}}{10} & 0 & -\frac{3\sqrt{2}}{10} & 0 & 0 \end{pmatrix} \quad (5)$$

where z is the normal to the quantum well, the function $U(z)$ depends only on jump in the semiconductor composition at the boundary. We have assumed it is a linear function of the Cd content x

$$U(z) = [1 - x(z)]g_4. \quad (6)$$

and g_4 is parameter of “mixing”.

The results of such calculation are presented in Fig. 9. We used the value $g_4 = 0.8 \text{ eV}\text{\AA}$ (the value $g_4 = 0.8 - 0.6 \text{ eV}\text{\AA}$ satisfactorily describes the experimental data on the splitting of the valence and conduction bands in the structures with $d \sim d_c$ [27]). Figure 9(b) shows that IIA leads to large (about 6–7 meV) “spin” splitting of the states in the valleys while the isoenergy contours of the upper states remain close to that calculated without IIA [compare Fig. 7 and Fig. 9(a)]. As Figs. 9(b) and 9(b) show, the splitting is so large that up to hole density of $\sim 4 \times 10^{12} \text{ cm}^{-2}$ the holes fill the upper split states only. Thus, taking into account the interface inversion asymmetry reduces the degeneracy of the top of valence band from 8 to 4 within studied hole density range. But this is not enough, because the experimental value of the degeneracy is 2.

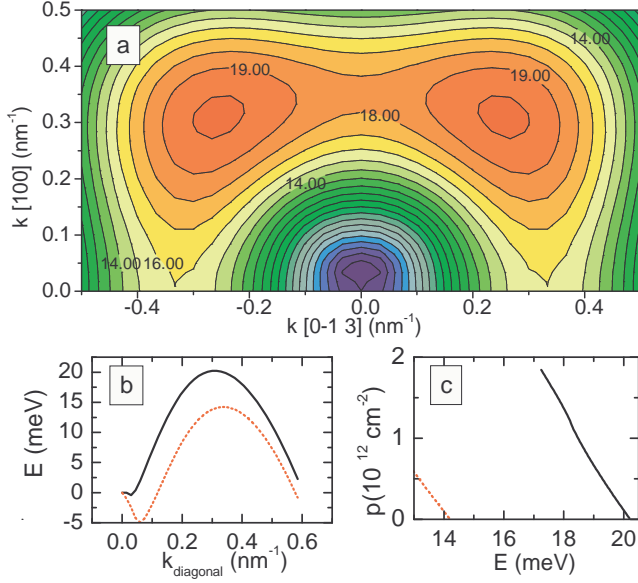


Figure 9. (Color online) (a) – The isoenergy contours of the upper split-off state calculated with taking into account IIA. (b) – The E versus k_{diagonal} dependences for both split-off states. (c) – The dependence of hole density in the upper (solid curve) and lower (dashed curve) split-off states on the Fermi energy.

What else does not take into account this theoretical model?

C. The role of the additional asymmetry of the quantum well resulting from difference of the mixing at the well boundaries and their broadening

In the previous section, we considered the role of mixing the states on the boundaries of a quantum well in the simplest symmetric case, when the additional term, Eq. (5), to the Hamiltonian is proportional to dU/dz and differs on the boundaries only by sign due to $x(z)$ [see Eq. (6)]. In this case, IIA removes the spin degeneracy, but leaves a valley degeneracy. As further calculations of the spectrum show, this state is unstable: the additional asymmetry of the boundary conditions, i.e. different values of the parameter g_4 at the boundaries, the different broadening of the walls of the quantum well lead to the removal of valley degeneracy, too. The reasons for this asymmetry relate to the fact that the walls of the quantum well are grown under different conditions (at different times and temperature). In addition, the electric field, normal to the 2D plane, both built-in, which results from uncontrolled doping of barriers, and created by a gate voltage, also leads to the removal of valley degeneracy.

As an example, in Fig. 10 we plot the results of the calculation of the spectrum with an insignificant difference in the parameter $g_4 = 1 \text{ eV\AA}$ and $g_4 = 0.8 \text{ eV\AA}$ for one and another boundaries (in Fig. 9, the value of parameter

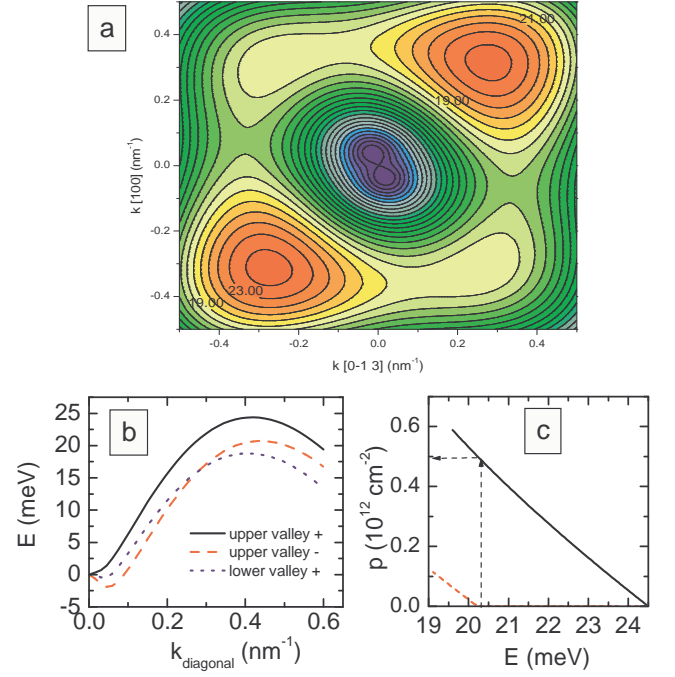


Figure 10. (Color online) (a) – The isoenergy contours of the upper split-off states calculated with the different parameter g_4 , namely $g_4 = 1 \text{ eV\AA}$ and $g_4 = 0.8 \text{ eV\AA}$ on one and another boundaries. (b) – The E versus k_{diagonal} dependences for both split-off states of upper valley (solid and dashed lines) and for upper states of lower valley (the dotted line). (c) – The dependence of hole density in the upper (solid curve) and lower (dashed curve) split-off states on the Fermi energy.

g_4 was equal to 0.8 eV\AA for both boundaries). A comparison of the isoenergy contours in Fig. 9(a) and Fig. 10(a) shows that such difference removes the valley degeneracy. As seen from Fig. 10(b) the “spin” splitting of the valleys practically unchanged, however the height of the valleys becomes different. This figure demonstrates, that within the Fermi energy range (24.5 – 20.5) meV, the holes fill only two from four “valleys”. This means that in this range, the degeneracy became 2 rather than 4. The dependence of the hole density on the Fermi energy presented in Fig. 10(c) shows that the degeneracy 2 should be up to the hole density of about $5 \times 10^{11} \text{ cm}^{-2}$. The arrow in this picture marks the energy when lower “valleys” begin to fill up that leads to increase of the rate dp/dE_F .

Thus, taking into account both the interface inversion asymmetry and difference in parameters of the wall of the quantum well allows us to explain the degeneracy of the top of valence band states [28]

Now consider the dependence of the holes effective mass on their density. The calculated dependences for the well with $d = 8.3 \text{ nm}$ for the two cases considered above are shown in Fig. 11. The solid curve shows the m_h versus p dependence calculated for the case when the parameter g_4 for both boundaries was equal to 0.8 eV\AA .

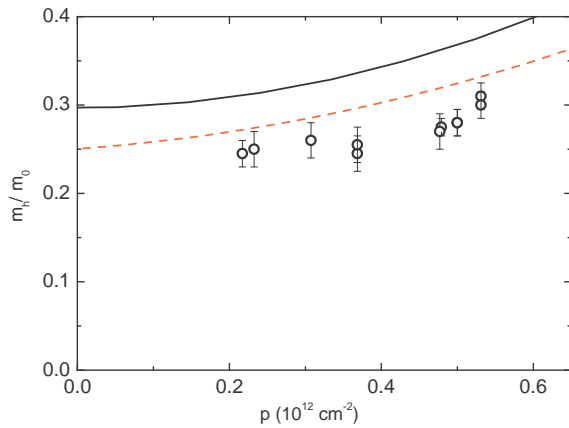


Figure 11. (Color online) The experimental (symbols) and theoretical (lines) hole density dependence of the hole effective mass in the structure with $d = 8.3$ nm. The solid line is calculated when the value of the parameter g_4 is the same for both boundaries of the quantum well, $g_4 = 0.8$ eVÅ. The dashed line is the case when the value of g_4 is different for different boundaries, $g_4 = 1$ eVÅ and 0.8 eVÅ.

The dashed curve is the case when $g_4 = 0.8$ eVÅ and 1 eVÅ for different boundaries. It can be seen that the values and the dependences on the density are quite close to each other. In this figure we present the experimental m_h values for the sample H1529 with $d = 8.3$ nm. They agree well with the calculated dependence for the second case.

Calculations carried out for wider wells, $d = (10 - 20)$ nm, show that taking into account only the difference in the parameter g_4 on the boundaries is not sufficient to remove the valley and spin degeneracy in the hole density range up to $p = (5 - 6) \times 10^{11} \text{ cm}^{-2}$ for which experimental results were presented in Fig. 6.

However, the calculations carried out within some modifications of the theoretical model which take into account other causes of asymmetry, the difference in broadening of the boundaries of the well, the electric field, normal to the 2D plane, show that it is possible to obtain the sufficient values of the spin and valley splitting. This is achieved with reasonable values for the parameters: the boundaries broadening is always less than $0.1d$, the electric field is less than $\simeq 6 \times 10^5$ V/cm, and $g_4 = (0.6 - 1.2)$ eVÅ. Therewith, the range of change of the effective mass, which is shown by the wide semi-transparent line in Fig. 6, is not wide and well describes the data obtained in all the structures investigated. It is currently not possible to separate the roles of various

mechanisms.

IV. CONCLUSION

We presented the experimental results of the studies of the longitudinal and transverse magnetoresistance in HgTe/Cd_xHg_{1-x}Te quantum wells of $(8.3 - 20.4)$ nm nominal width in the hole conductivity regime in a wide range of hole density. Comparison of the Hall density with the density found from the period of the SdH oscillations clearly shows that the degeneracy of states of the top of the valence band is equal to 2 over the entire hole density range from $1 \times 10^{11} \text{ cm}^{-2}$ to $5.5 \times 10^{11} \text{ cm}^{-2}$. This value of the degeneracy does not agree with the calculations of the spectrum performed within the framework of the 4-bands kP -method for symmetric quantum wells. These calculations show that the top of the valence band consists of four spin-degenerate extremes located at $k \neq 0$, which gives the total degeneracy $K = 8$. It is shown that taking into account the mixing of states at the interfaces [29] leads to the removal of the spin degeneracy, which reduces the degeneracy to $K = 4$. However, such a state is unstable. Taking into account any additional asymmetry (the difference in the mixing parameters at the interfaces, the different broadening of the boundaries of the well, etc.) leads to the removal of valleys degeneracy, making $K = 2$ within the investigated range of hole density. It is noteworthy that for our case two-fold degeneracy occurs due to degeneracy of two single-spin valleys.

Another parameter of the energy spectrum, the hole effective mass, was experimentally determined in the entire range of the hole density by analyzing the temperature dependence of the amplitude of the SdH oscillations. We have shown that the effective mass at $p \simeq 2 \times 10^{11} \text{ cm}^{-2}$ in the wells of width $d = (8 - 20)$ nm is equal to $(0.25 \pm 0.02) m_0$ and weakly increases with the increasing hole density. Such a value of m_h and its dependence on p are in a good agreement with the calculated effective mass of the valleys.

ACKNOWLEDGMENTS

We are grateful to E.L. Ivchenko and M. Nestoklon for useful discussions. The work has been supported in part by the Russian Foundation for Basic Research (Grants No. 16-02-00516, No. 15-51-06001 and No. 15-02-02072), by Act 211 Government of the Russian Federation, agreement No. 02.A03.21.0006, and by the Ministry of Education and Science of the Russian Federation under Project No. 3.9534.2017/BP.

¹ Q. N. Yafei Ren, Zhenhua Qiao, Rep. Prog. Phys. **79**, 066501 (2016).

² L. G. Gerchikov and A. Subashiev, Phys. Stat. Sol. (b) **160**, 443 (1990).

- ³ X. C. Zhang, A. Pfeuffer-Jeschke, K. Ortner, V. Hock, H. Buhmann, C. R. Becker, and G. Landwehr, *Phys. Rev. B* **63**, 245305 (2001).
- ⁴ E. G. Novik, A. Pfeuffer-Jeschke, T. Jungwirth, V. Latussek, C. R. Becker, G. Landwehr, H. Buhmann, and L. W. Molenkamp, *Phys. Rev. B* **72**, 035321 (2005).
- ⁵ B. A. Bernevig, T. L. Hughes, and S.-C. Zhang, *Science* **314**, 1757 (2006).
- ⁶ M. Zholudev, Ph.D. thesis, University Montpellier 2, France (2013).
- ⁷ S. A. Tarasenko, M. V. Durnev, M. O. Nestoklon, E. L. Ivchenko, J.-W. Luo, and A. Zunger, *Phys. Rev. B* **91**, 081302 (2015).
- ⁸ G. Landwehr, J. Gerschütz, S. Oehling, A. Pfeuffer-Jeschke, V. Latussek, and C. R. Becker, *Physica E* **6**, 713 (2000).
- ⁹ X. C. Zhang, A. Pfeuffer-Jeschke, K. Ortner, C. R. Becker, and G. Landwehr, *Phys. Rev. B* **65**, 045324 (2002).
- ¹⁰ K. Ortner, X. C. Zhang, A. Pfeuffer-Jeschke, C. R. Becker, G. Landwehr, and L. W. Molenkamp, *Phys. Rev. B* **66**, 075322 (2002).
- ¹¹ X. C. Zhang, K. Ortner, A. Pfeuffer-Jeschke, C. R. Becker, and G. Landwehr, *Phys. Rev. B* **69**, 115340 (2004).
- ¹² M. König, S. Wiedmann, C. Brüne, A. Roth, H. Buhmann, L. W. Molenkamp, X.-L. Qi, and S.-C. Zhang, *Science* **318**, 766 (2007).
- ¹³ G. M. Gusev, Z. D. Kvon, O. A. Shegai, N. N. Mikhailov, S. A. Dvoretzky, and J. C. Portal, *Phys. Rev. B* **84**, 121302 (2011).
- ¹⁴ Z. D. Kvon, E. B. Olshanetsky, E. G. Novik, D. A. Kozlov, N. N. Mikhailov, I. O. Parm, and S. A. Dvoretzky, *Phys. Rev. B* **83**, 193304 (2011).
- ¹⁵ D. A. Kozlov, Z. D. Kvon, N. N. Mikhailov, S. A. Dvoretzky, and J. C. Portal, *Pis'ma Zh. Eksp. Teor. Fiz.* **93**, 186 (2011), [*JETP Lett.* **93**, 170 (2011)].
- ¹⁶ Z. D. Kvon, S. N. Danilov, D. A. Kozlov, C. Zoth, N. N. Mikhailov, S. A. Dvoretzky, and S. D. Ganichev, *Pis'ma Zh. Eksp. Teor. Fiz.* **94**, 895 (2011), [*JETP Letters* **94**, 816 (2011)].
- ¹⁷ G. M. Minkov, A. V. Germanenko, O. E. Rut, A. A. Sherstobitov, S. A. Dvoretzky, and N. N. Mikhailov, *Phys. Rev. B* **88**, 155306 (2013).
- ¹⁸ E. Olshanetsky, Z. Kvon, N. Mikhailov, E. Novik, I. Parma, and S. Dvoretzky, *Solid State Commun.* **152**, 265 (2012).
- ¹⁹ N. N. Mikhailov, R. N. Smirnov, S. A. Dvoretzky, Y. G. Sidorov, V. A. Shvets, E. V. Spesivtsev, and S. V. Rykhlitski, *Int. J. Nanotechnology* **3**, 120 (2006).
- ²⁰ I. M. Lifshits and A. M. Kosevich, *Zh. Eksp. Teor. Fiz.* **29**, 730 (1955), [*Sov. Phys. JETP* **2**, 636 (1956)].
- ²¹ It should be noted that the $1/B_{min}$ versus N dependence extrapolates to zero at $N = 0$. It does not mean that the Berry phase is equal to zero. In 2D systems in which carrier density, but not the Fermi energy, is constant with the growing magnetic field, the $1/B_{min}$ versus N dependence extrapolates to zero at $N = 0$ regardless of the value of the Berry phase.
- ²² M. S. Zholudev, A. V. Ikonnikov, F. Teppe, M. Orlita, K. V. Maremyanin, K. E. Spirin, V. I. Gavrilenko, W. Knap, S. A. Dvoretzky, and N. N. Mihailov, *Nanoscale Research Letters* **7**, 534 (2012).
- ²³ K. Takita, K. Onabe, and S. Tanaka, *Phys.Stat. sol. b* **92**, 297 (1979).
- ²⁴ Note that all the calculations of the Landau levels, performed until now (see, e.g., Ref. [4, 30]), inadequately describe the behavior of the Landau levels of the valence band in weak magnetic fields for quantum wells with $d > (7 \sim 8)$ nm. It is easy to understand if we take into account the following considerations. The valence band top in these quantum wells is realized in the side valleys where the effective electron mass is negative. Therefore, in weak magnetic fields Landau levels should move down with increasing magnetic field. However, the calculations presented in the literature [4, 30] show the movement of the Landau levels upwards.
- ²⁵ Such discrepancy forced the authors of [17] to use the isotropic approximation for analysis of the experimental data. At this approximation the valleys are absent and isoenergy contours are concentric circles. However, in this case, the values of the hole effective mass differ significantly from theoretical ones.
- ²⁶ X. Dai, T. Hughes, X. Qi, Z. Fang, and S. Zhang, *Phys.Rev. B* **77**, 125319 (2008).
- ²⁷ G. M. Minkov, A. V. Germanenko, O. E. Rut, A. A. Sherstobitov, M. O. Nestoklon, S. A. Dvoretzky, and N. N. Mikhailov, *Phys. Rev. B* **93**, 155304 (2016).
- ²⁸ It should be noted that the degeneracy two for our case is valley degeneracy of two single-spin valleys. However "spin" states of these valleys are different therefore the magnetic field should split LL due to the Zeeman effect. We assume the distortion of the SdH oscillations at $B > 2.5$ T evident from Fig. 3(a) is result of such splitting. At $B < 2.5$ T the Zeeman splitting is small and does not lead to splitting of the SdH oscillations.
- ²⁹ E. Ivchenko, *Optical spectroscopy of semiconductor nanostructures* (Alpha Science International, Harrow, UK, 2005) p. 427.
- ³⁰ M. König, H. Buhmann, L. W. Molenkamp, T. Hughes, C.-X. Liu, X.-L. Qi, and S.-C. Zhang, *Journal of the Physical Society of Japan* **77**, 031007 (2008).